Iterative suppression of Kerr-induced instabilities in Bessel beams using on-axis intensity shaping

Ismail Ouadghiri-Idrissi[1] and François Courvoisier[1,*]
[1] FEMTO-ST Institute, Univ. Franche-Comté, CNRS, 15B avenue des Montboucons, 25030 Besançon cedex, France.
[*] francois.courvoisier@femto-st.fr

This article has been published in open access in *Optics Continuum*.
Its full reference is:
"Iterative suppression of Kerr-induced instabilities in Bessel beams using on-axis intensity shaping"
I. Ouadghiri-Idrissi and F. Courvoisier, Opt. Continuum, 3, 379-385 (2024) https://doi.org/10.1364/OPTCON.512110

Kerr-induced instabilities in zeroth-order Bessel beams with low focusing angle prevent the formation of longitudinally uniform plasma rods in the filamentation regime. These instabilities lead to the oscillation of the beam on-axis intensity via the generation of new spatial frequencies by a first stage of spectral broadening followed by a second stage of four-wave mixing. Here, we numerically demonstrate an efficient approach to drastically reduce the instabilities due to the second stage. It is based on shaping the longitudinal intensity profile with spatio-spectral components in opposition of phase to the Kerr-generated ones via an iterative approach. Zeroth-order Bessel beams with a longitudinal flat intensity plateau can be generated in a few iterations in the nonlinear regime. This is performed in both monochromatic and pulsed femtosecond regimes.

1 Introduction

Bessel beams are a special class of diffraction-free beams which are solutions to Helmholtz equation in free space [1] with a longitudinally invariant intensity profile. A zeroth-order Bessel beam is characterized by a cylindrically-symmetric amplitude profile $\sim J_0(k_r^0 r)$ and has a Fourier spectrum centered around the spatial frequency $k_r^0 = 2\pi/\lambda \sin\theta$. λ is the laser wavelength and θ is the *cone angle*, *i.e.* the angle of the corresponding geometrical rays with the optical axis [1,2]. Bessel beams can be also called conical beams, because of the conical structure of their wavevectors. Since an ideal Bessel beam carries infinite energy, it cannot be realized physically. Approximate, finite-energy versions of Bessel beams were introduced, such as Bessel-Gauss beams. In the linear regime, the spatial spectrum of the beam determines the evolution of the on-axis intensity along the propagation. A top-hat ring distribution of the spatial frequencies, as in reference [1] produces a Bessel beam with strong on-axis oscillations because of the sharp edges of the k_r distribution. In contrast, a Gaussian spectrum produces the Bessel-Gauss beam that can be produced with a perfect axicon [2]. Because of the properties of the Fourier transform, the spectral width is inversely proportional to the Bessel beam length [2,3]. Importantly, it is possible to shape the spatial spectrum and fully control the on-axis intensity pattern, such as generating a flat plateau or a linear ramp over a fixed distance [4]. These beams, in the linear regime, have found a wide range of

applications such as imaging [5], or optical trapping [6].

Of particular interest, Bessel beams can also preserve the propagation-invariant property even in the nonlinear and filamentation regimes [7]. This invariance is very advantageous in high-power laser applications such as materials processing [8–13], terahertz radiation generation [14,15], plasma waveguide generation [16], electric discharge guiding [17] where long and uniform laser-generated plasma rods are required. However, this steady filamentation regime can only be obtained for specific experimental conditions [7] where nonlinear absorption is high enough.

In the case of low focusing conditions, Bessel beams sustain nonlinear instabilities, induced by Kerr nonlinearity, which lead to the modulation of their central core intensity along propagation [18–20]. The instability is due to the generation by the Kerr effect of two spatial frequencies that interfere with the original Bessel beam.

References [19,21] have shown that instability grows in two stages. In the first stage, the beam undergoes an initial Kerr spectral broadening, leading to the generation of an axial wave "seed" (defined at a spatial frequency $k_r \approx 0$). In the second stage, this axial wave seed intervenes as a signal wave in Kerr-induced four-wave mixing (FWM) processes, leading to its amplification and the generation of an outer ring in the frequency space at spatial frequencies around $k_r \approx \sqrt{2}k_r^0$.

The nonlinear instabilities are highly detrimental for all applications requiring uniform plasma rods. Here, we aim to reduce their growth to obtain a Bessel beam with uniform on-axis intensity over a long propagation distance. Recently, we have shown that these instabilities can be reduced if the Bessel beam is progressively formed inside the Kerr medium and explained results in terms of spectral phase distribution of the input beam [22]. The best intensity growth profile found is the parabolic increase. Yet this technique is efficient, we show in [21] that this method only allows damping the nonlinear growth of the first stage. The nonlinear growth still occurs for longer propagation distances. In Fig. 1(a), the blue solid curve is the target on-axis intensity profile with a parabolic increase followed by a flat intensity plateau. The nonlinear regime is shown in Fig 1(b) (solid blue curve), and we see that oscillations start growing on the plateau. (We note that the amplitude of these oscillations is already several times less than the oscillations generated in a Bessel-Gauss beam with comparable intensity and length). The parabolic increase of intensity reduces the efficiency of the first nonlinear stage, *i.e.* the spectral broadening. It leads to inefficient FWM interactions for a relatively short propagation distance. However, if the Bessel extent is relatively long, FWM interactions will become more efficient and nonlinear instabilities will thus be inevitably enhanced.

In this paper, we report a concept that allows us to directly decrease the efficiency of FWM interactions, so as to maintain a uniform intensity plateau even in the nonlinear regime. Our aim is to ensure the most uniform beam before other nonlinear effects arise, such as nonlinear ionization, *i.e.,*for intensities typically below $\sim$ 50 TW.cm^{-2}in fused silica. As discussed above, nonlinear oscillations of the on-axis intensity of Bessel beams are the result of the interference of the input conical beam with the self-generated spectral components [20], and specifically the outer ring with spatial frequency $\sqrt{2}k_{r0}$. Our

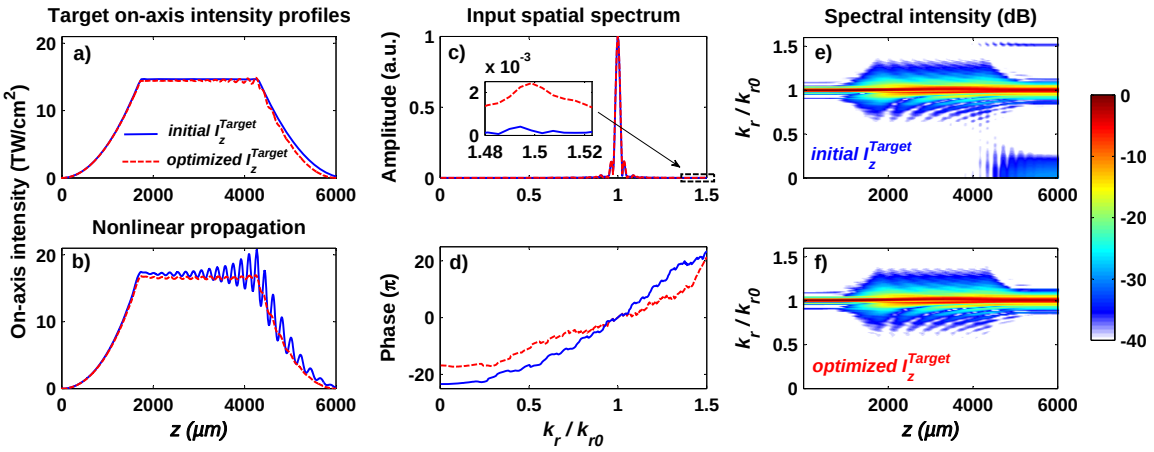

Figure 1: Comparison of initial (blue solid lines) and optimized (red dashed lines) Bessel beams. (a) targeted on-axis intensity profiles I_z^{Target}: the initial profile is in the form of parabolic ramps on both sides of a flat plateau and optimized profile after six iterations (see main text). (b) Evolution of the central core intensity along propagation (on-axis intensity) in the Kerr nonlinear regime described by Eq.1; (Middle column) Comparison of the input spectral distribution (c) and input phase (d) of Bessel beams with the initial and optimized profiles. (Third column) Evolution along propagation of the spectral intensities (in dB) as a function of the spatial frequency k_r/k_{r0} for (e) the initial beam and (f) the optimized beam.

approach is based on linearly creating, by beam shaping, a spatial frequency component in opposition of phase to the Kerr-induced one. In direct space (by opposition to the spatial frequency space), the input on-axis intensity profile of the new Bessel beam exhibits oscillations in the linear propagation regime. We will use an iterative approach to adjust the phase and amplitude of these oscillations to match those produced by Kerr nonlinearity.

2 Algorithm

To implement our approach, we start by simulating the nonlinear propagation of a Bessel beam with a flat intensity plateau and recording the profile of the corresponding on-axis intensity in the nonlinear regime. Then, we design a modified Bessel beam with an optimized on-axis intensity profile: it has the same form as the original, but presents an oscillating behavior with the same oscillation period as that obtained in the nonlinear regime in opposition of phase. For the beam shaping, we use the approach described in Ref. [23], which establishes the link between the input profile with a target on-axis intensity $I(z)$. Then, we simulate the nonlinear propagation of this axially-shaped Bessel beam. Actually, a complete suppression of these nonlinear intensity oscillations cannot happen using a single shaping step. This is because a variation in the on-axis intensity leads to a variation in the intensity of Kerr-generated waves, affecting the resulting nonlinear modulation. In this regard, we propose an iterative algorithm for repeating the above-described steps until the depth of nonlinear intensity modulation is decreased under a chosen threshold. We will first describe our approach using the monochromatic approximation and then extend our work to ultrafast pulses.

Our numerical simulations are based on nonlinear Schrödinger equation developed for cylindrically-symmetric coordinate as in Ref. [22] for monochromatic approximation:

$$\frac{\partial A}{\partial z} = \frac{i}{2\,k}\Delta_{\perp}A + i\,k\frac{n_2}{n_0}|A|^2 A \tag{1}$$

where $A \equiv A(r,z)$ is the envelope of an electric field $E = Re[A\exp(-i\omega_0 t + i\,k\,z)]$; $\omega_0 = 2\pi c/\lambda$ and k denote the angular frequency and wavevector defined for wavelength λ. $\Delta_{\perp}$ is the transverse Laplacian, $r = \sqrt{x^2+y^2}$, t and z are the radial, temporal and propagation coordinates.

The input spatial envelope $A(r, z=0)$ is computed using the approach of Ref. [23]. We evaluate the spatial spectrum $\tilde{A}(k_r, z=0)$ corresponding to a given on-axis intensity profile I_z^{Target} according to:

$$\tilde{A}(\sqrt{k^2-k_z^2}, z=0) = \frac{1}{k_z}\int_{-\infty}^{+\infty}\sqrt{I_z^{\mathrm{Target}}}\exp\left[i\,(k_{z0}-k_z)\,z\right]\mathrm{d}z \tag{2}$$

where $k_z = \sqrt{k^2-k_r^2}$ is the longitudinal spatial frequency and $k_{z0} = k\cos(\theta)$ (θ is the cone angle *i.e.,* the angle of the wavevectors with the optical axis). Then $A(r, z=0)$ is computed using inverse Hankel transform of $\tilde{A}(k_r, z=0)$.

The results shown in Fig. 1 are obtained for an on-axis intensity plateau of $I_{\max} = 14.5$ TW/cm^2. The other numerical parameters are presented in table 1 and correspond to propagation in fused silica.

Our optimization procedure is briefly described in Algorithm 1 where I_z^{Target} and I_z^{NL} are respectively the target intensity profile (linear regime) and its corresponding nonlinear on-axis intensity profile. Both are defined for a given iteration "j". The goal of this algorithm is to minimize the nonlinear on-axis modulation depth, denoted I_z^{err}, which characterizes the growth of new spectral components. We define this parameter as $I_z^{\mathrm{err}} = \frac{\max(I_z^{\mathrm{NL}})-\min(I_z^{\mathrm{NL}})}{2\,\mathrm{mean}(I_z^{\mathrm{NL}})}$. We set a minimal value η of this parameter under which the iterations end. Note that, we minimize I_z^{err} over a limited propagation range, *i.e* over the distance where we target obtaining a flat intensity plateau.

The target on-axis intensity profile I_z^{Target} is optimized after each iteration: it preserves the same profile as the initial one while its oscillation depth is changed to be the opposite of that obtained in the nonlinear regime of the previous iteration. In fact, for the algorithm to converge, we do not correct the full amplitude of the oscillations, but instead, we correct only a fraction α of the difference between target and nonlinear regime intensity profiles ($0 < \alpha < 1$). Here, we worked with typically $\alpha < 0.3$.

Table 1: **Numerical parameters used in simulations.**

λ (μm)	θ ($^\circ$)	n_0	n_2 (m^2/W)
0.8	4	1.46	$2.48\,10^{-20}$

Algorithm 1 Optimization of on-axis intensity profile

procedure OPTIMIZ($I_z^{\mathrm{Target}}, I_z^{\mathrm{NL}}, \eta$) ▷ correcting I_z^{Target} using I_z^{NL}
  for $j = 1 : N_j$ **do** ▷ N_j maximal number of iterations
    $I_z^{\mathrm{NL}}(j) \leftarrow$ nonlinear propagation of $I_z^{\mathrm{Target}}(j)$
    $I_z^{\mathrm{err}} = \frac{\max(I_z^{\mathrm{NL}}) + \min(I_z^{\mathrm{NL}})}{2\,\mathrm{mean}(I_z^{\mathrm{NL}})}$ ▷ in high-intensity z-range
    if $I_z^{\mathrm{err}} > \eta$ **then** ▷ η target minimal error rate
      $I_z^{\mathrm{Target}}(j+1) \leftarrow I_z^{\mathrm{Target}}(1)[1 + \alpha(I_z^{\mathrm{Target}}(1) - I_z^{\mathrm{NL}}(j))]$
      ▷ $I_z^{\mathrm{Target}}(j)$ & $I_z^{\mathrm{NL}}(j)$ normalized; $0 < \alpha < 1$
    else save $I_z^{\mathrm{Target}}(j)$
      return
    end if
  end for
end procedure

3 Results in the monochromatic approximation

Figure 1 shows a first set of simulation results comparing the initial and optimized beams after six iterations. We choose a minimal error rate η of 5%, which we aim to obtain in the flat-top propagation zone of the initial target profile. Optimized target profiles are computed after each iteration for a fixed value of $\alpha = 0.25$. In Fig.1(a), the solid blue line is the initial, non-optimized intensity profile, which consists of parabolic rise, flat-top, and parabolic decay. The other profile (red dash line) is the optimized profile, i.e. exhibiting small on-axis oscillations that were engineered in the optimization process. The nonlinear propagation of these two Bessel beams is shown in Fig.1(b). It is apparent that the nonlinear modulation is significantly reduced for the optimized Bessel beam. The maximal oscillation depth has been spectacularly decreased from 17.2 % to only 0.2 % of the intensity plateau. This corresponds to a reduction of 99 % of the oscillation amplitude on an already optimized profile.

Figures 1(c) and (d) show respectively the spatial spectral amplitude and phase of the two input profiles. While the general amplitude spectrum is mostly unchanged, the inset shows the addition of a spectral component at $k_r \approx 1.5k_{r0}$ in the amplitude distribution of the optimized beam. This is the component that cancels the effect of the Kerr-generated ones in the FWM process. Figures 1(e) and (f) show respectively the evolution of initial and optimized beam spatial spectra with propagation distance. While the axial wave and outer ring are clearly visible in the initial case from 4000 μm propagation distance, they have disappeared below -40 dB for the optimized case.

In Fig. 2 we show another example with a higher value of the intensity plateau $I_{\max}$ for which Kerr-induced processes are more efficient than for lower intensities. With the same error rate, fifteen iterations are needed to decrease the error below the target value. We show a sample of the different on-axis intensity profiles in the nonlinear regime to show the progressive reduction of the oscillations. Here, we used a varying value of α such that it is decreasing after each iteration in the range $[0.145 - 0.28]$. Note that the target error rate could not be obtained in case a fixed value of α was used even for a higher

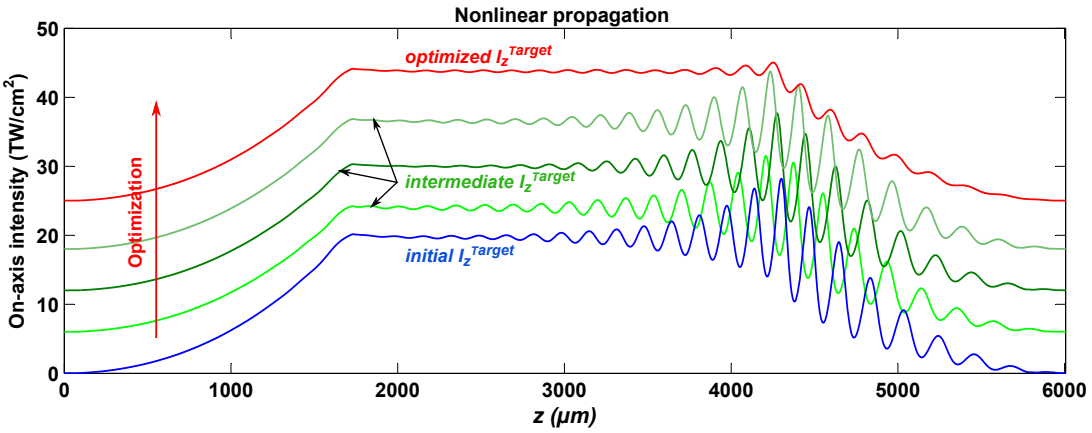

Figure 2: Optimization of the on-axis intensity profile of a Bessel beam with higher intensity plateau $I_{\max} = 16.5$ TW/cm^2) in fifteen iterations to obtain nonlinear modulation depth lower than the target value $\eta = 5\ \%$. The plot shows the intensities of the nonlinear regime for five cases. For better readability, the plots were vertically spaced by 6 TW.cm^{-2}, and only three of 14 intermediate steps are shown. The progressive reduction of the oscillations is apparent.

number of iterations. These results show that as the Kerr nonlinearity increases, it becomes difficult to compensate for the growth of nonlinear instabilities.

We have also considered a different initial on-axis profile, as in the case of an initial linear ramp before the flat plateau. Using the same parameters as Fig. 1, the corresponding Bessel beam undergoes strong nonlinear instabilities leading to a modulation depth $I_z^{\rm err}$ reaches about 400 $\%$ [22]. Our optimization decreases it by a factor more than 10, to about 35 $\%$ (Figure not shown), but we cannot decrease it further down. Hence, for overall optimal results, it is preferable to start the optimization from an on-axis intensity profile, for which Kerr instabilities only grow from the second stage.

4 Extension to the femtosecond pulsed regime

Our approach can also be extended for ultrashort pulses. To establish a proof-of-principle, we use the same algorithm described above and define the on-axis intensity I_z as the maximal intensity in the time domain. (Note that in the case of pulse splitting, the maximal intensity will temporally shift from the central time of the pulse). We define the input spatio-temporal spectrum as follows:

$$\tilde{A}(\sqrt{k^2-k_z^2},\omega,z=0)=\frac{\exp\left[-i\left(\omega-\omega_0\right)^2 t_p^2/4\right]}{k_z(\omega)} \times\int_{-\infty}^{+\infty}\sqrt{I_z^{\mathrm{Target}}}\exp\left[i\left(k_{z0}-k_z\right)z\right]\mathrm{d}z \tag{3}$$

where we consider an input Gaussian temporal envelope with a radius t_p defined at $1/e$ of its maximal amplitude.

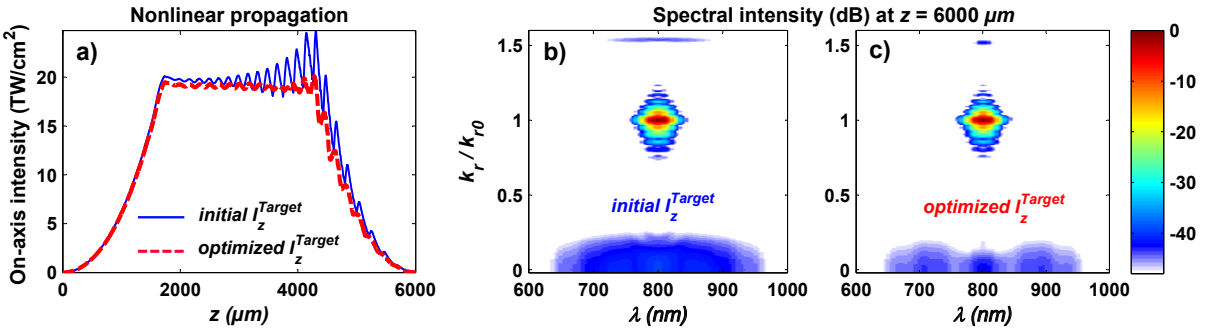

Figure 3: Proof of principle extension to a pulsed regime. a) Optimization of the peak temporal on-axis intensity profile of a modified Bessel beam ($I_{\max} = 16.5$ TW/cm^2) in two iterations to obtain nonlinear modulation depth lower than $\eta = 5.2$ %. (solid line) initial beam and (dashed line) final iteration. Comparison of their respective (b and c) spatio-temporal spectra at a propagation distance of $z = 6000\,\mu m$.

In our simulations, we consider a femtosecond Bessel beam ($t_p = 105$ fs) with the same parameters as in Fig. 2. We compare in Fig. 3(a) the temporal peak intensity along propagation for the initial and optimized I_z^{Target}. We obtain a minimal error rate $\eta = 5.2\%$ after only two iterations. Figures 3(b) and (c) show respectively the spatio-temporal spectra of the initial and optimized pulse at the end of the propagation ($z = 6000$ μm). We observe that the spectral broadening of both the axial wave and outer ring is substantially reduced in the optimized case.

5 Conclusion

To summarize, we reported a proof-of-principle method to reduce nonlinear instabilities in both monochromatic and pulsed Bessel beams along their propagation. Our method is based iteratively on compensating for the growth of the Kerr-induced spatio-spectral component around $\sim \sqrt{2}k_{r0}$ by adding to the input beam an identical component such that is in opposition of phase. This is performed via on-axis intensity shaping that is experimentally possible using the approach demonstrated in Ref [4]. Although not shown here, we have also confirmed the validity of the approach for ultrashort Bessel beams even when nonlinear absorption is considered. Obviously, increasing the number of control parameters, such as allowing

the independent shaping of all temporal frequencies is expected to provide even better results. Further investigations are worth performing to improve the optimization process and control of Kerr-induced effects encountered in the time domain (such as self-phase modulation), also in the presence of time-delayed Raman contributions to the nonlinear Kerr effect. The essence of this control approach could be further enhanced using machine-learning strategies [24]. We believe our approach will increase the applicability of Bessel beams in many fields of applications and can be extended to other beams.

Funding

H2020 European Research Council (ERC) (682032-PULSAR). Agence Nationale de la Recherche EIPHI Graduate School (ANR-17-EURE-0002). Conseil Régional de Bougogne Franche-Comté.

Disclosures

The authors declare no conflicts of interest.

Data availability

Data underlying the results presented in this paper are not publicly available at this time but may be obtained from the authors upon reasonable request.

1. Durnin, J. Exact solutions for nondiffracting beams. I. The scalar theory. *Journal of the Optical Society of America A* **4**, 651 (1987).

2. Jarutis, V., Paškauskas, R. & Stabinis, A. Focusing of Laguerre–Gaussian beams by axicon. *Optics Communications* **184**, 105–112 (2000).

3. Vetter, C. *et al.* Realization of free-space long-distance self-healing Bessel beams. *Laser Photonics Rev.* **13**, 1900103 (2019).

4. Ouadghiri-Idrissi, I. *et al.* Arbitrary shaping of on-axis amplitude of femtosecond Bessel beams with a single phase-only spatial light modulator. *Optics Express* **24**, 11495 (2016).

5. Fahrbach, F. O., Simon, P. & Rohrbach, A. Microscopy with self-reconstructing beams. *Nature Photonics* **4**, 780–785 (2010).

6. Garcés-Chávez, V., McGloin, D., Melville, H., Sibbett, W. & Dholakia, K. Simultaneous micromanipulation in multiple planes using a self-reconstructing light beam. *Nature* **419**, 145–147 (2002).

7. Polesana, P., Franco, M., Couairon, A., Faccio, D. & Trapani, P. D. Filamentation in kerr media from pulsed Bessel beams. *Physical Review A* **77**, 043814 (2008).

8. Amako, J., Sawaki, D. & Fujii, E. Microstructuring transparent materials by use of nondiffracting ultrashort pulse beams generated by diffractive optics. *Journal of the Optical Society of America B* **20**, 2562 (2003). URL http://dx.doi.org/10.1364/JOSAB.20.002562.

9. Bhuyan, M. K. *et al.* High aspect ratio nanochannel machining using single shot femtosecond Bessel beams. *Appl. Phys. Lett.* **97**, 081102 (2010). URL http://dx.doi.org/10.1063/1.3479419.

10. Duocastella, M. & Arnold, C. Bessel and annular beams for materials processing. *Laser & Photonics Reviews* **6**, 607–621 (2012). URL http://dx.doi.org/10.1002/lpor.201100031.

11. Courvoisier, F., Stoian, R. & Couairon, A. Ultrafast laser micro- and nano-processing with non-diffracting and curved beams. *Optics & Laser Technology* **80**, 125–137 (2016).

12. Bergner, K. *et al.* Scaling ultrashort laser pulse induced glass modifications for cleaving applications. *Appl. Opt.* **57**, 5941 (2018).

13. Meyer, R. *et al.* Extremely high-aspect-ratio ultrafast Bessel beam generation and stealth dicing of multi-millimeter thick glass. *Applied Physics Letters* **114**, 201105 (2019).

14. Bitman, A., Moshe, I. & Zalevsky, Z. Improving depth-of field in broadband THz beams using nondiffractive Bessel beams. *Optics Letters* **37**, 4164 (2012).

15. Ardaneh, K. *et al.* Femtosecond laser-induced sub-wavelength plasma inside dielectrics. III. terahertz radiation emission. *Physics of Plasmas* **30** (2023).

16. Durfee, C. G. & Milchberg, H. M. Light pipe for high intensity laser pulses. *Physical Review Letters* **71**, 2409–2412 (1993).

17. Clerici, M. *et al.* Laser-assisted guiding of electric discharges around objects. *Science Advances* **1**, e1400111 (2015).

18. Andreev, N. E., Aristov, Y. A., Polonskii, L. Y. & Pyatnitskii, L. N. Bessel beams of electromagnetic waves: self-effect and nonlinear structures. *Zhurnal Eksperimentalnoi i Teoreticheskoi Fiziki* **100**, 1756–1766 (1991).

19. Gadonas, R. *et al.* Self-action of Bessel beam in nonlinear medium. *Optics Communications* **196**, 309–316 (2001).

20. Polesana, P. *et al.* Observation of conical waves in focusing, dispersive, and dissipative Kerr media. *Physical Review Letters* **99**, 223902 (2007).

21. Ouadghiri-Idrissi, I., Dudley, J. M. & Courvoisier, F. Control of spatial four-wave-mixing efficiency in Bessel beams using longitudinal intensity shaping. *Physical Review A* **100**, 043804 (2019).

22. Ouadghiri-Idrissi, I., Dudley, J. M. & Courvoisier, F. Controlling nonlinear instabilities in Bessel beams through longitudinal intensity shaping. *Optics Letters* **42**, 3785 (2017).

23. Čižmár, T. & Dholakia, K. Tunable Bessel light modes: engineering the axial propagation. *Optics Express* **17**, 15558 (2009).

24. Genty, G. *et al.* Machine learning and applications in ultrafast photonics. *Nature Photonics* **15**, 91–101 (2020).